Hindawi
Advances in Materials Science and Engineering
Volume 2023, Article ID 9826891, 1 page
https://doi.org/10.1155/2023/9826891

Retraction

Retracted: Experimental and Thermal Investigation on Powder Mixed EDM Using FEM and Artificial Neural Networks

Advances in Materials Science and Engineering

Received 26 December 2023; Accepted 26 December 2023; Published 29 December 2023

This article has been retracted by Hindawi, as publisher, following an investigation undertaken by the publisher [1]. This investigation has uncovered evidence of systematic manipulation of the publication and peer-review process. We cannot, therefore, vouch for the reliability or integrity of this article.

Please note that this notice is intended solely to alert readers that the peer-review process of this article has been compromised.

Wiley and Hindawi regret that the usual quality checks did not identify these issues before publication and have since put additional measures in place to safeguard research integrity.

We wish to credit our Research Integrity and Research Publishing teams and anonymous and named external researchers and research integrity experts for contributing to this investigation.

The corresponding author, as the representative of all authors, has been given the opportunity to register their agreement or disagreement to this retraction. We have kept a record of any response received.

References

[1] V. N. R. Jampana, P. S. V. Ramana Rao, and A. Sampathkumar, "Experimental and Thermal Investigation on Powder Mixed EDM Using FEM and Artificial Neural Networks," *Advances in Materials Science and Engineering*, vol. 2021, Article ID 8138294, 12 pages, 2021.

Hindawi
Advances in Materials Science and Engineering
Volume 2021, Article ID 8138294, 12 pages
https://doi.org/10.1155/2021/8138294

Research Article

Experimental and Thermal Investigation on Powder Mixed EDM Using FEM and Artificial Neural Networks

Venkata N. Raju Jampana,[1] **P. S. V. Ramana Rao**,[1] **and A. Sampathkumar**[2]

[1]*Centurion University of Technology and Management, Visakhapatnam, Andhra Pradesh, India*
[2]*Dambi Dollo University, Dembi Dolo, Ethiopia*

Correspondence should be addressed to A. Sampathkumar; dr.sampathkumar@dadu.edu.et

Received 14 July 2021; Revised 14 August 2021; Accepted 19 August 2021; Published 6 September 2021

Academic Editor: Samson Jerold Samuel Chelladurai

Electric discharge machining (EDM) process is one of the earliest and most extensively used unconventional machining processes. It is a noncontact machining process that uses a series of electric discharges to remove material from an electrically conductive workpiece. This article is aimed to do a comprehensive experimental and thermal investigation of the EDM, which can predict the machining characteristic and then optimize the output parameters with a newly integrated neural network-based methodology for modelling and optimal selection of process variables involved in powder mixed EDM (PMEDM) process. To compare and investigate the effects caused by powder of differently thermo physical properties on the EDM process performance with each other as well as the pure case, a series of experiments were conducted on a specially designed experimental setup developed in the laboratory. Peak current, pulse period, and source voltage are selected as the independent input parameters to evaluate the process performance in terms of material removal rate (MRR) and surface roughness (Ra). In addition, finite element method (FEM) is utilized for thermal analysis on EDM of stainless-steel 630 (SS630) grade. Further, back propagated neural network (BPNN) with feed forward architecture with analysis of variance (ANOVA) is used to find the best fit and approximate solutions to optimization and search problems. Finally, confirmation test results of experimental MRR are compared using the values of MRR obtained using FEM and ANN. Similarly, the test results of experimental Ra also compared with obtained Ra using ANN.

1. Introduction

The process of PMEDM is known as the appropriate abrasive material mixing with the powder formatted metallic material into the dielectric fluid, where the powder particles (i.e., electrically conductive) are amalgamated in the dielectric fluid that mitigates the insulating strength of particles and enhances the distance of spark gap between the workpiece and tool for uniform distribution of electric discharge in all the directions. This is also referred as new advancement to get better innovations and enhancement in the potentialities of EDM process [1]. This process is more static, i.e., highly stable, and results in enhanced MRR and smoothened surface [2, 3]. In addition, EDM process is also called as thermal erosion procedure [4]. During the process of machining, there will be a change in the machining surface layer physical properties due to the instantaneous rise in the temperature, which also results in the residual stress presence. This is the main factor that influences the surface quality of machining and its functional performance. In addition, the properties of component are also influenced by thermal residual stresses with higher magnitude, which are formed on the surface of workpiece upper layer because of speedy curing of EDM process [5, 6]. Usually, utilization of components in EDM occurs at certain circumstances such as higher temperature, stress, and fatigue-load, which results in significant mitigation in component's fatigue life. Hence, it is required to utilize powder mixing methods, which do not need any posttreatment procedure to find the optimized machining parameters of EDM, which also suppress the cracks formation in the recast layer for maximum life even under various fatigue-loads. The dilation of enough powder

particles to the dielectric in EDM results in enhanced quality in the surface finishing with maximum speed of machining compared to the classical EDM process (without powder mixing). Standard dielectric circulation device employed in PMEDM is illustrated in Figure 1, which is installed in the setup of traditional EDM operational tank. It also comprises with a micropump or stirrer, which is used to prevent the settling of powder particles at the dielectric reservoir bottom, and it also assists to keep the powder particles on the workpiece surface from stagnating. There are some permanent magnets (shown in blue color) distributed by the filtering device to insulate the debris from the particles of powder.

1.1. Powder-Based Parameters

1.1.1. Type of Powder. Generally, MRR and surface durability improves, and instrument wear rate reduces by adding the dielectric powder. Further, the efficiency of processes has impacted distinctly by these sorts of powders. Some of the effected parameters are nonmagnetic characteristics, thermal conductivity, suspension capabilities, and electric conductivity. Inorganic oxide powders are not considered as the better output characteristics due to the even distribution of dielectric powder.

1.1.2. Powder Size. In machined surface quality, an influential parameter is additive particle size [7]. The higher interelectrode gap is resulted for larger particles based on the analyzation of experimental results. It leads to the lower deionization between tool and workpiece and greater contamination. The gap increases by the larger powder size, but MRR is reduced, and Ra is increased [8].

1.1.3. Powder Conductivity. The discharge gap increases by adding the conductive fine powder electrically in dielectric that enhances spark frequency and improves debris flushing [7]. From the interelectrode gap, heat with large amount is confiscated by forming the shallow crates on the surface of workpiece due to the higher thermal conductivity of these particles [9, 10].

1.1.4. Powder Concentration. Due to the enhancement of number of discharges by powder concentration, which improves MRR [11], surface roughness is decreased while lowering the energy per spark [12]. An optimum powder concentration is needed with the consistent increment in concentration which improves the amount of powder particles in the discharge gap. The discharge energy transfer impedes to the workpiece and arching and short-circuiting while reducing the surface and quality of MRR [13].

1.1.5. Powder Density. The surface forces affect the powder particle density that has allowed the particle distribution in the dielectric uniformly. These forces could balance by the lower density and requirement of powder quantity is reduced due to the reduction of settling down of powder amount at the tank bottom [14].

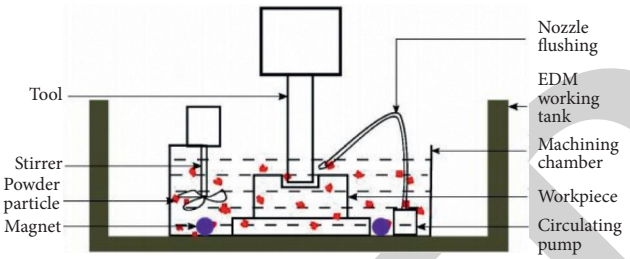

Figure 1: PMEDM setup.

2. Related Work

Surekha et al. [15] have studied aluminium powder added EDM for EN-19 alloy steel machining based on a brass electrode and disclosed that peak current (I_p) and gap voltage (V_G) parameters have impacted the values of MRR. In [16], Tahsin et al. have examined Ti6A14V ELI material PMEDM for analysing the effect of powder concentration of SiC on the surface topography, subsurface structures, and particle deposition. The material transfer mechanism improves the suspended particle concentration and lowers the pulse currents. Because of secondary discharges scarcity, the depletion of current material transfer mechanism has performed at higher pulse rate. Selvarajan et al. [17] reviewed EDM with different industrial demanded composite materials and demonstrated various parameters that effect on the performance. Choudhury et al. [18] have focused on investigation on the hybrid PMEDM using the powders of multiwalled carbon nanotube (CNT) and aluminium that mixed in kerosene for machining the EN-19 alloy steel with brass electrode. Kumar et al. [19] have tested the machinability of Inconel 825 with addition of graphene nanopowder to the die sinking EDM dielectric fluid. For creating the conditions of optimum process, the methodology of response surface (RSM) is exploited. The impact of input process parameters such as I_p, pulse on time (T_{ON}), and V_G on output response features like MRR, Ra, and TWR was also examined. Later, the Inconel-800 machinability using PMEDM has been investigated [20], where the experimental designs and optimization have performed using desirability approach and RSM. The most effected metrics for MRR included tool material, T_{ON}, and I_p while powder materials, tool material, T_{ON}, and I_p for TWR. Mishra and Routaray [21] have focused on achieving the objective of correlating the thermally induced hardness of workpiece impact with EDM performances and the modified property establishes that is responsive for the deviation change in the output responses behaviour in sinking the process of electrical discharge machining. Based on four controllable input parameters such as V_G, pulse of time (T_{OFF}), T_{ON}, and I_p, the RSM has implemented using central composite design approach for experimental comparative study. Here, the desired response variables were chosen as the energy density, TWR, and MRR. The changes in output responses such as energy density, TWR, and MRR have affected

predominantly through the observation of hardness change based on the process of base alloy induction thermal hardening. Sidhu and Yazdani [22] have evaluated for predicting the optimal machining conditions in the particular-reinforced metal matrix composites (30 vol%Sic/A359) EDM. In [23], the authors have investigated the chromium powder effect that mixed with EDM surface features of alloy tool steel SKD11. The chromium content increases on machined surface if chromium powder concentration is high and discharge current is low. Ekmekci et al. [24] have proposed a substitute realistic technique to generate the coating or biocompatible interfaces for medical applications. While processing the Ti6A14V EDM, combination of deionized water and hydroxyapatite (HA) powder has been used as a dielectric fluid. Khazraji et al. [25] studied the impact of parameters on copper and graphite electrodes when PMEDM is processed using RSM. For graphite and copper electrodes, the total percentage of heat has increased by adding micropowders of SiC into dielectric fluid. However, the generated heat is higher compared to the used kerosene dielectric. The improvement of 110% and 124% has been achieved with the use of same kerosene dielectric and electrodes in WLT, respectively. In [26], the authors have tested the input variable effect on TWR, MRR, and overcut size during PMEDM of AISI 1045, H11 die steel, and HCHCr. Kerosene and commercial EDM oil have been used as dielectric fluids with three powders such as tungsten, graphite, and silicon and brass, graphite, and tungsten as electrodes. Based on the results, TWR reduced and MRR and overcut size increased with powder concentration. Kuriachen et al. [27] have studied the SiC microparticle effect that mixed to dielectric media on Ti6A14V machining with tungsten carbide electrode. The statistical design of RSM-Box Behnken has been proposed and the process variables effect was tested such as powder concentration, capacitance, and voltage over machining features such as TWR and MRR using variance analysis. At minimum levels of powder concentration and middle levels of voltage and capacitance, maximum MRR has been obtained and minimum TWR attained at minimum levels of voltage, capacitance, and powder concentration. Baseri et al. [28] have studied the effect of TiO_2 nanopowder on EDM rotary tool of H13. The input parameters of tool rotation speed, spark energy, and powder concentration percentage influence on the responses such as Ra, TWR, and MRR. Based on the integration of rotational tool and nanopowder, the EDM efficiency has been improved. S. Tripathy and D. K. Tripathy [29] studied the parameters such as I_p, V_G, powder concentration, T_{ON}, and duty cycle and their impact on machining characteristics such as TWR, EWR, MRR, and Ra with the addition of chromium powder to the dielectric fluid in EDM. The adaption of Taguchi method integrated with this technique also demonstrated for preference order as similar as ideal solution. For PMEDM of H11 die steel, optimization of multiple performance characteristics has been discussed using the copper electrode. The optimum process conditions have been obtained and the reduced Ra was observed on improving the chromium powder concentration. Recently, the impact on molybdenum disulphide powder that is mixed to dielectric medium during micro-EDM of Inconel 718 is studied [30]. The results have shown that the MRR has maximized at powder optimum size, i.e., 50 nm. In [31], SS630 grade of EDM process is investigated and optimized using Taguchi approach, where flushing pressure, T_{ON}, T_{OFF}, and I_p are assumed as input process variables. The output performance has been measured with MRR and Ra. Further, optimization was also done using Taguchi approach by assuming L_{16} orthogonal array with Minitab software. However, it is important to make a note that SS630 content based on PMEDM has not been analysed in the literature. The stainless-steel substance SS630 is extremely hard to do machining due to the factors such as high corrosive resistance, high build-up edge propensity, and poor thermal conductivity. However, the product applications in different industries such as pharmaceutical industries, pump production, and other device prototypes and, in addition, several recent works focused on optimization of process parameters using fuzzy networks [32] and artificial neural networks [33–35]. Therefore, this article proposes an experimental and thermal investigation with process parameter optimization using BPNN with feed forward architecture on PMEDM for SS630 using SiC powder as dielectric fluid. In addition, copper tungsten (CuW) is selected as the tool electrode owing to the copper which is a high conductive element electrically. Instead of kerosene, EDM oil is used as a dielectric substance due to the unfortunate environmental and other external conditions.

2.1. Proposed Methodology. In the current experimental study, EDM is considered to carry out the experiments with CuW cylinder tool electrode, which has a diameter of 10 mm, and we tested the dielectric flow system that was modified for suspended dielectric medium of SiC powder circulation in small quantities for preventing the whole dielectric fluid contamination. SS630 is chosen as a workpiece with the size of $70 \times 40 \times 8$ mm. The input parameters are selected as concentration of SiC powder, servo voltage, I_p, and T_{ON} using 18 experiments with three factors and three levels of factorial design experiments.

3. Materials and Methods

The SS630 material is chosen for workpiece that has thickness of 8 mm and rectangular dimensions of 70×40 mm. At lower temperatures, a single ageing treatment can harden to reduce the risk of distortion using this SS630 as workpiece. In addition, if corrosion and high strength are required, then grade 630 is an ideal selection for the experimental analysis. A mixture of tungsten and copper is used for electrode material of CuW, where the distinct particles of one metal have included material that dispersed in a matrix of the other one as tungsten and copper are not soluble mutually. It has a length of 21.5 mm and a diameter of 12.5 mm. Tables 1 and 2 show the chemical composition and material properties for both workpiece and electrodes, respectively.

Table 1: Chemical composition of SS630 material.

Element	Weight (%)
Carbon (C)	0.036–0.44 Max
Manganese (Mn)	0.60–1.00 Max
Silicon (Si)	0.40 Max
Chromium (Cr)	16.00–18.00
Nickel (Ni)	10.00–14.00
Molybdenum (Mo)	2.00–3.00
Phosphorus (P)	0.05 Max
Sulphur (S)	0.030 Max
Nitrogen (N)	0.10 Max
Iron (Fe)	Balance

SiC powder has a set of unique physical-chemical properties such as large bandwidth, high resistance to oxidation and corrosion, low coefficient of thermal expansion, excellent thermal conductivity, high hardness, and mechanical stability at higher temperatures. The chemical composition of SiC is demonstrated in Table 3.

3.1. Performance Measurements. This section describes the performance measurements utilized in PMEDM process of SS630, where both MRR and SR have been used as an output performance validation. Here, the mean absolute deviation is measured from the average surface level to obtain the value of Ra (in μm) based on a computer-controlled Ra tester. By using the removed volume of material per unit time, MRR is computed because it is a crucial parameter that shows effect on the productivity and processing time of EDM machining. The definition of MRR is described as the ratio between pre- and postmachining weight difference of workpiece and the multiplication of workpiece density and machining time, which is formulated as follows:

$$\text{MRR} = \frac{W_b - W_a}{\rho_w \times t} \times 1000\,\text{mm}^3/\text{min}, \quad (1)$$

where W_b and W_a (in gm) denote the weight of workpiece before and after machining process, respectively; ρ_w denoted as the workpiece material density which is 7750 kg/m^3 for SS630 grade; and t is the processing time of machining, i.e., 5 mins.

3.2. Modelling and Simulation of the Heat Flux Using FEM. For all EDM and PMEDM models, the feasibility of problem is obtained by considering the following assumptions to overcome the issues of EDM such as random, uncertainty, and high complexity nature:

(1) Workpiece and tool material properties are relied on temperature
(2) Transient type of temperature analysis is considered
(3) Heat source is assumed as the heat flux Gaussian distribution on the workpiece material surface during T
(4) The channel of EDM discharge spark is considered as a uniform shape of cylindrical column
(5) Not effecting the element shape and density
(6) Isotropic and homogeneous characteristics of workpiece materials
(7) Considering an axisymmetric model
(8) Heat flux incident magnitude on the electrodes is not depending on the affected surface profile
(9) The diameter of a channel would be between 10 μm and 100 μm and the electrode can be considered as a semiinfinite body

3.3. ANN Model. For modelling complex nonlinear relationships between variables, ANNs are used as an intelligent tool that mimics the work process as a nervous system. It contains a network of artificial neurons that can learn the complicated relationship between input variables such as T_{ON}, machining time, I, and source voltage (V_S) and output variables such as MRR and Ra. First, we designed a set of experiments and fed to relevant ANN model that can model the interrelation between input and output variables. The outcome of the settled dataset machining parameter that provided to ANN model is predicted using this model and it is categorized into two sets known as testing and training datasets. For neural network training, the dataset of training is used while the prediction of model accuracy is verified using the testing dataset.

4. Experimental Setup

This section describes the experimental setup process that carried out the analysis on effects of one or more factors of parameters on the machined surface finish by focusing on determining the effect of input process parameters such as T_{ON}, T_{OFF}, I, and V_S. Performance evaluation of all the experiments has been done using the die sinking EDM machine of FORMATICS 50 model equipped with ELECTRONICA PRS 20, as shown in Figure 2. Before the process of machining, the electrode surfaces and workpieces are polished and cleaned. Tables 4 and 5 are listed with the selected input factors and their corresponding levels and selected experimental conditions, respectively. On the machined surfaces, the Ra is computed based on the tester of Talysurf surface roughness, which is computed transversely with the consideration of cut-off length as 0.8 mm and the process is repeated for three times for estimating the average values.

4.1. Thermal Investigation Using FEM. For estimating both molten material deformations by plasma pressure and temperature distribution, the commercial finite element code ANSYS is incorporated for EDM in the single discharge analysis procedure. To determine solutions for engineering problem, finite element code is used by ANSYS. The complex interaction of various physical phenomena is involved in EDM which is a complicated thermal process. Thus, FEM is employed for simulating the stress and temperature distributions into the workpiece, where a powerful software like ANSYS is needed for improving the FEM-based EDM model

Table 2: Typical properties of commonly used copper tungsten compositions.

Composition	Density (g/cm^3≥)	Hardness (kgf/mm^2)	Resistivity ($\mu\Omega$·cm)
W50/Cu50	11.85	115	3.2

Table 3: Chemical composition of SiC.

SiC	Silicon carbide
Density	3.21 g/cm³
Molecular weight/molar mass	40.11 g/mol
Melting point	2,730°C
Thermal conductivity	3 W m-k
Specific heat	1800 j/kg-k

Figure 2: Machining process of PMEDM.

Table 4: Input process parameters and their levels.

Parameter	Level 1	Level 2	Level 3
C_p (%)	0	3	5
T_{ON} (μs)	8	12	16
T_{OFF} (μs)	15	22	30
I_p (Amps)	6	10	14
V_S (Volts)	3	4	5

with the consideration of all complicated aspects of process. It can be used with different models and analyses any complicated geometry that includes different capabilities of FEM ranging from a linear, simple, and static analysis to a nonlinear, complex, and transient dynamic analysis in the structural mechanics, electromagnetic and thermal systems, and fluid mechanics.

Here, ANSYS 14.5 software has been utilized to simulate the results for PMEDM modelling by creating the work geometry through the appropriate boundary constraints and applying different types of loads. The mapped meshing technique is used for meshing the workpiece domain. As mentioned earlier, SS630 and CuW are utilized as specimens for a single discharge set. Figure 3 depicts the temperature distribution obtained for I_p = 14 A with T = 750 μs, where the distribution of temperature is maximum at the end of workpiece and minimum at the middle of workpiece, i.e., 100°C and 22.001°C, respectively. After the distribution of temperature, the heat flux is computed and plotted, as shown in Figure 4, where the maximum heat flux is 1.7577 W/mm^2 at the workpiece end region and the minimum heat flux is 0.1553 W/mm^2 at the middle region of workpiece. The structural error is disclosed in Figure 5, with the maximum and minimum MRR of 0.01209 mJ and 0.0013343 mJ at the end region and middle region of workpiece, respectively.

Table 5: Experimental conditions.

Working condition	Description
Workpiece	SS630 grade (70 × 40 × 8 mm)
Electrode	CuW (diameter 12.5 mm and length 21.5 mm)
Dielectric	SiC powder
Polarity	Normal
Gap voltage	70 V
Machining time	5 mins

5. Results and Discussion

5.1. Calculation of Analytical MRR (A-MRR). To estimate the removed material amount from specimen, temperature profile is used that has been obtained from FEM and to form circular parabolic geometry, crater is formed owing to each discharge. The paraboloid geometry is used to define the theoretical crater volume as formulated below:

$$V_c = \frac{1}{2} \times \pi \times S \times R_c^2, \tag{2}$$

where S represents the depth; R_c is the crater radius; V_c (FEM) is the volume, and 3D points contained in V_c represent the points over liquid temperature; and S and R_c values are obtained by estimating the temperature distributions over depth and radius directions of workpiece.

5.2. Calculation of Experimental MRR (E-MRR). MRR is described as the quotient value of division of pre- and postmachining weight difference and density and time of workpiece machining. It is defined as follows:

$$\text{MRR} = \frac{W_b - W_a}{\rho_w \times t} \times 1000\,\text{mm}^3/\text{min}, \tag{3}$$

where ρ_w indicates the density of workpiece; t is the machining processing time; and W_b and W_a represent the before and after machining workpiece weight. Table 6 is listed with the obtained values of A-MRR, T-MRR, and Ra with varying the input process variables using FEM and

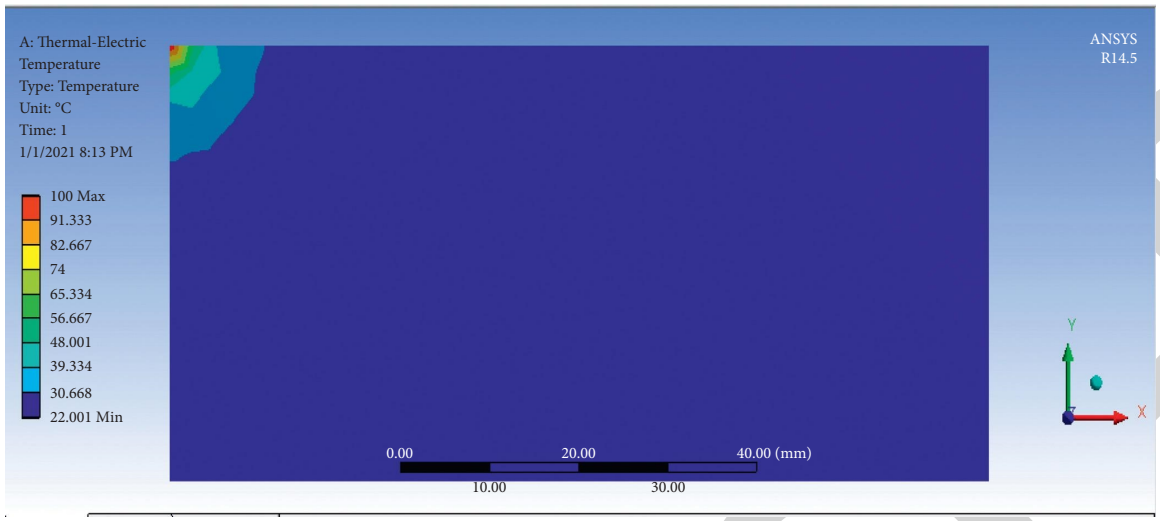

Figure 3: Temperature distribution obtained for a current intensity value of 14 A and pulse duration 750 μs.

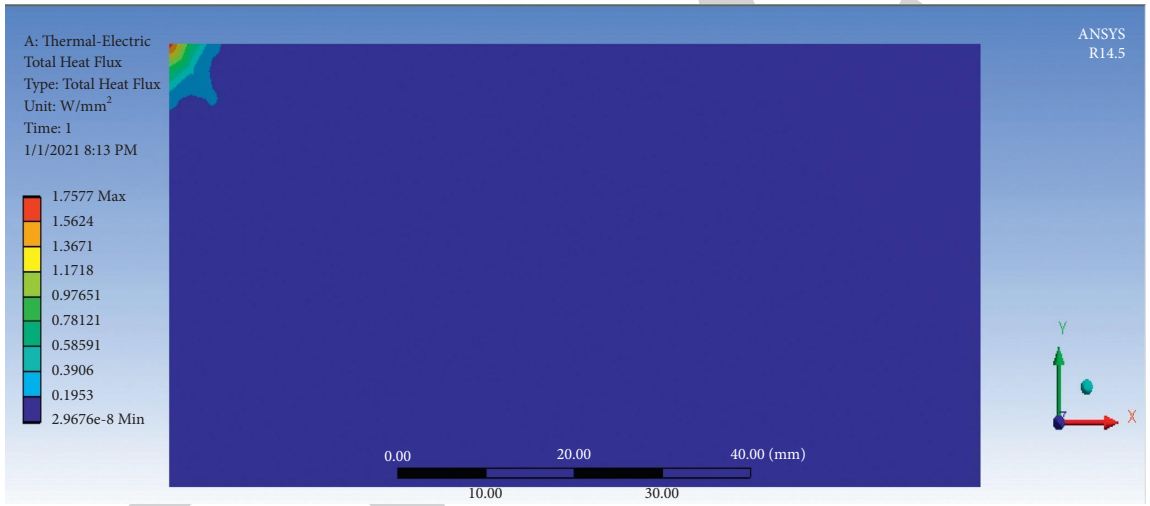

Figure 4: Volume of material removed for current intensity value of 14 A and pulse duration 750 μs.

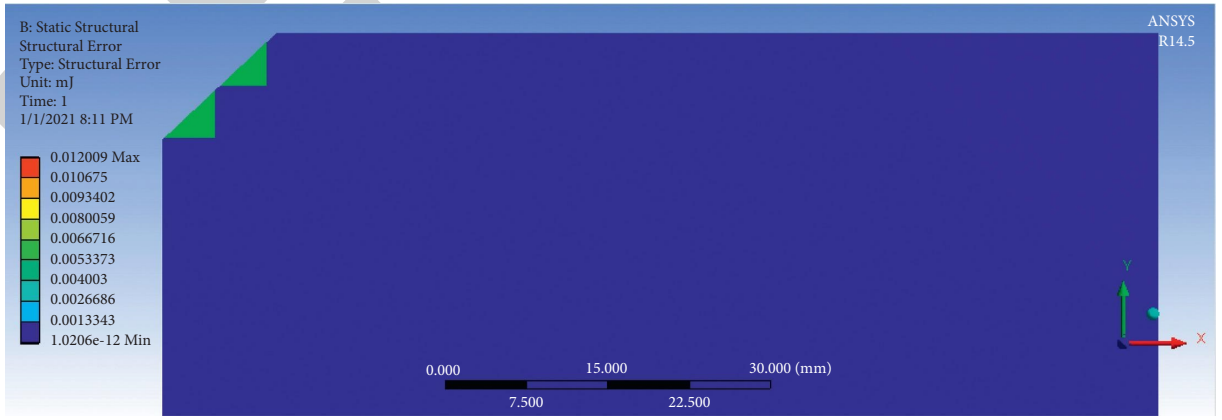

Figure 5: Structural error.

experimentally for the PMEDM process of SS630. In addition, the performance comparison graph of A-MRR and E-MRR is demonstrated in Figure 6.

5.3. Reasons for Deviation in Values of A-MRR and E-MRR. Practically, some deviations are noticed in the values of A-MRR compared to the E-MRR, which is due to some

Table 6: Obtained values of A-MRR, E-MRR, and Ra.

S. No.	C_p	T_{ON}	T_{OFF}	I_p	V_s	A-MRR (mm^3/min)	E-MRR (mm^3/min)	Ra (μm)
1	0	8	15	6	3	1.914	2.145	2.932
2	0	12	22	10	4	2.562	2.986	2.381
3	0	16	30	14	5	5.142	5.008	5.142
4	3	8	15	10	4	2.154	2.256	2.461
5	3	12	22	14	5	4.521	4.469	2.594
6	3	16	30	6	3	3.941	3.997	5.173
7	5	8	15	6	5	3.842	4.120	2.196
8	5	12	22	10	3	4.641	4.976	3.868
9	5	16	30	14	4	5.814	5.896	3.790
10	7	8	15	14	4	3.910	4.139	2.542
11	7	12	22	6	5	3.143	3.245	3.481
12	7	16	30	10	3	4.963	4.897	2.896
13	9	8	15	14	3	4.144	4.245	2.760
14	9	12	22	6	4	3.794	3.986	2.749
15	9	16	30	10	5	5.903	6.113	1.695
16	12	8	15	10	5	3.943	3.876	3.521
17	12	12	22	14	3	5.304	5.436	3.987
18	12	16	30	6	4	3.949	4.103	2.612

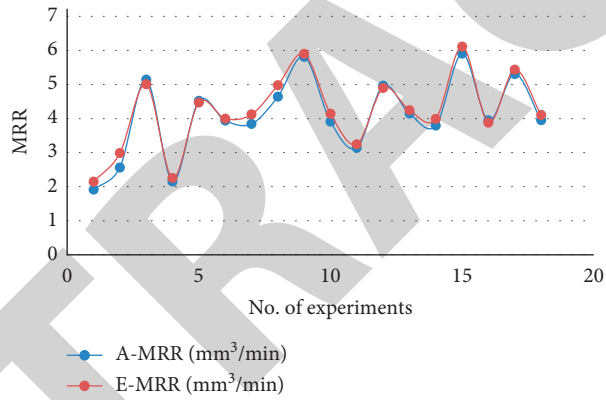

Figure 6: Performance comparison graph of A-MRR and E-MRR.

simplifying assumptions such as no ignition delays while machining, hundred percent material flushing efficiency, and not depositing the recast layer in the workpiece after machining. The flushing of melted workpiece materials is not done fully from the crater and a considerable number of melted materials is solidified in the crater again and formed the recast layer. The realization of ideal machining conditions is not done because of improper debris flushing those results in arching into the interelectrode gap while processing the machining of high energy discharges and reduced the actual value of MRR. Due to the parameters such as spark gap, sensitivity, dielectric fluid, and lift medium, the MRR is affected. In addition, an important role is played by dielectric fluid medium as it comes into picture for convection only, but it is essential to consider during machining process. By vaporizing and melting the material, the material removal is caused from the workpiece mainly. The dielectric material is taken away by the molten metal, but the molten metal is under heavy pressure owing to the plasma channel. Moreover, the material removal problem arises from workpiece due to the adhesive property of molten metal. However, it is a tough task to design the model with the inclusion of all practical effects to the analytical model.

5.4. ANOVA. For each control factor, ANOVA is required to be estimated for accessing the factors impact on response. To investigate which design parameters effect the characteristic significantly, the experimental results have been assessed using the method of ANOVA, which can identify the input parameter contributions on Ra and MRR. To detect the process parameters whose variance in the design space impacts the output response metrics, ANOVA is applied while choosing 90% of confidence interval for experimental investigation. If the computed probability (p) value is about 10% or less, the factor significance is considered. After ANOVA, the obtained value of p is demonstrated in Table 7 and their significance on output response metrics such as Ra and MRR, respectively.

5.5. Regression Analysis. After the process of PMEDM, the regression analysis is conducted based on the obtained data

Table 7: Major factors and corresponding p values for PMEDM process.

Model	p value	
Factor	Ra	MRR
A	0.086	0.062
B	0.072	0.007
C	0.079	0.097
D	0.048	0.054
E	0.022	"Insig"
AB	0.075	0.030
AC	0.015	"Insig"
AD	0.063	"Insig"
AE	"Insig"	0.010
BC	"Insig"	0.056
DE	0.062	0.029
ABC	0.047	0.096
ADE	"Insig"	"Insig"

results and the linear equations are derived that are relevant to the dependent and independent variables, which is performed using Minitab software and the regression equations are as follows:

$$Ra = 12.39 + 7.02A + 2.08B + 0.978C - 3.23D - 8.96E - 0.016AB + 0.0146AC - 0.311AD - 0.81AE - 0.0751BC + 0.802DE - 0.0088ABC + 0.0383ADE, \quad (4)$$

$$\text{E} - \text{MRR} = -5.18 - 7.22A - 1.06B - 0.66C + 1.83D + 5.31E + 0.027AB + 0.0129AC + 0.431AD + 1.04AE + 0.0560BC - 0.445DE + 0.0045ABC - 0.0768ADE. \quad (5)$$

Based on the listed values of R^2, Adj-R^2, and Pred-R^2 in Table 8, the potency of equations (4) and (5) can be realized for predicting the variance inside the design space. After employing ANOVA, the derived model equations have been found out for estimating the variability within the design space for all output responses based on the results analyzation.

5.6. Modelling of Proposed Feed Forward BPNN. Figure 7 shows the block diagram of the proposed scalable conjugate gradient-based feed forward BPNN, where the input process variables such as C_p, I, V_S, T_{ON}, and T_{OFF} are given as input to the proposed 5-10-2 architecture of feed forward BPNN, as shown in Figure 8, which consists of single input layer, hidden layer, and output layer. The input layer contains 5 nodes that represent C_p, I, V_S, T_{ON}, and T_{OFF} as input nodes. The hidden layer consists of 10 nodes that are denoted as hidden nodes and the output layer consists of two nodes, i.e., MRR and Ra as output nodes. Two stages are involved in the proposed PMEDM process modelling, i.e., testing and training of network using experimental machining data. The values for T_{ON}, T_{OFF}, I, V_S, C_p, Ra, and MRR have been included in the training dataset. Such types of 96 datasets have been used, out of which 82 were randomly chosen and utilized for training purpose in case of SiC powder added EDM while remaining 14 datasets presented for training the network as new application data to test and validate the network model predictive accuracy. Hence, the data which had not been used for training are used to evaluate the network. The predicted MRR and Ra are compared with the target values of MRR and Ra, i.e., E-MRR and E-Ra. Final optimized values of P-MRR and P-Ra will be computed based on the weight's adjustment, which reduces the error values.

5.6.1. Data Preprocessing. It is essential to perform the experimental data into patterns before the training of NN and mapping learnt. An input condition vector P_i is used to create the training and test pattern vectors where it contains C_p, T, I, and V_S and the corresponding target vector T_i, which consists of MRR and Ra. It is an important thing to consider the input and output data scale specifically in case of different operating ranges for process parameters. Without any skewing variable results, the ANN will be trained effectively by ensuring the scaling or normalizing. In the training, all input parameters are equally important, and each term is mapped to a value between −1 and 1 based on the following formula of linear mapping:

$$N = \frac{(R - R_{\min}) \times (N_{\max} - N_{\min})}{(R_{\max} - R_{\min})} + N_{\min}, \quad (6)$$

where N is the normalized value of the real variable; $N_{\max}$ and $N_{\min}$ refer to the normalization minimum and maximum values, respectively; and $R_{\min}$ and $R_{\max}$ are the minimum and maximum values of real variable while R is the real variable. Table 9 demonstrates the comparison of obtained output responses such as MRR and Ra using experimentation and prediction which are denoted as P-MRR and P-Ra. The performance comparison graph of obtained

Table 8: Residuals for all performance parameters.

	Ra	MRR
R^2	0.9124	0.9154
Adj-R^2	0.8962	0.9015
Pred-R^2	0.8824	0.8408

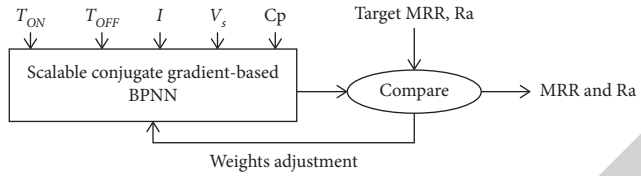

Figure 7: Proposed block diagram of scalable conjugate gradient-based feed forward BPNN.

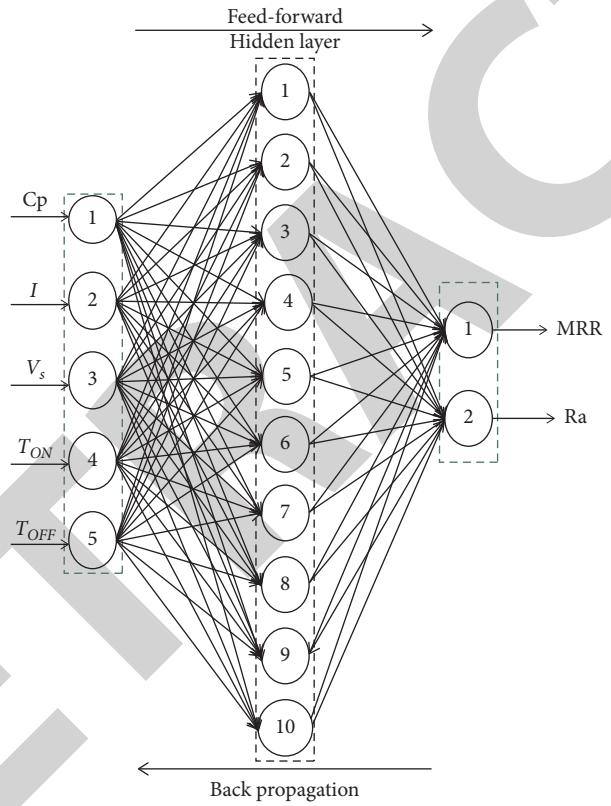

Figure 8: Proposed 5-10-2 architecture of feed forward BPNN.

Table 9: Comparison of E-MRR and E-Ra with optimized values predicted using ANN model, i.e., P-MRR and P-Ra.

S. No.	C_p	T_{ON}	T_{OFF}	I_p	V_S	E-MRR (mm³/min)	P-MRR (mm³/min)	E-Ra (μm)	P-Ra (μm)
1	0	8	15	6	3	2.145	2.301	2.932	2.910
2	0	12	22	10	4	2.986	2.820	2.381	2.112
3	0	16	30	14	5	5.113	5.092	5.142	5.231
4	3	8	15	10	4	2.256	2.457	2.461	2.568
5	3	12	22	14	5	4.469	4.134	2.594	2.448
6	3	16	30	6	3	3.997	3.896	5.173	5.198
7	5	8	15	6	5	4.120	4.110	2.196	2.019
8	5	12	22	10	3	4.976	4.954	3.868	3.782
9	5	16	30	14	4	5.896	5.784	3.790	3.793

Table 9: Continued.

S. No.	C_p	T_{ON}	T_{OFF}	I_p	V_S	E-MRR (mm³/min)	P-MRR (mm³/min)	E-Ra (μm)	P-Ra (μm)
10	7	8	15	14	4	4.139	4.124	2.542	2.547
11	7	12	22	6	5	3.245	3.214	3.481	3.442
12	7	16	30	10	3	4.897	4.891	2.896	2.895
13	9	8	15	14	3	4.245	4.321	2.760	2.667
14	9	12	22	6	4	3.986	3.997	2.749	2.789
15	9	16	30	10	5	6.113	6.192	1.695	1.731
16	12	8	15	10	5	3.876	3.897	3.521	3.567
17	12	12	22	14	3	5.436	5.332	3.987	3.980
18	12	16	30	6	4	4.103	3.985	2.612	2.423

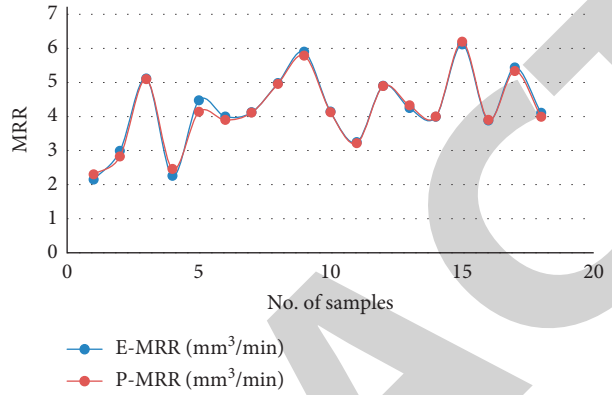

Figure 9: Performance comparison of obtained values of E-MRR and P-MRR for number of samples.

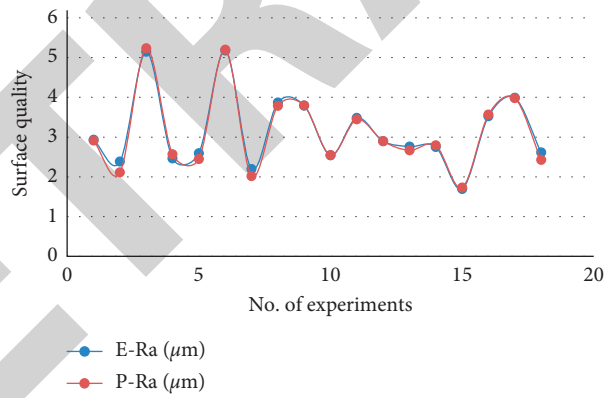

Figure 10: Performance comparison of obtained values of E-Ra and P-Ra for number of samples.

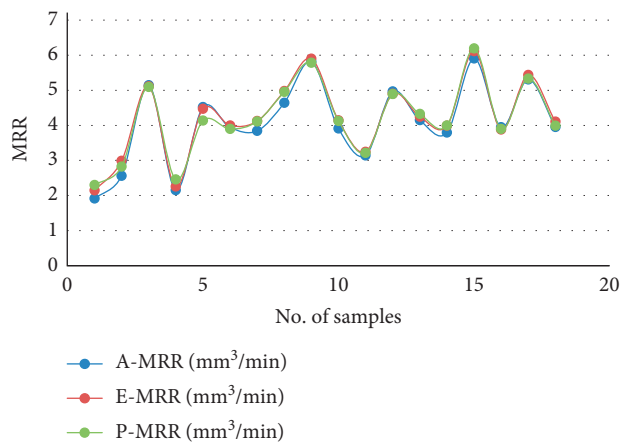

Figure 11: Performance comparison graph of MRR using FEM and experimental and feed forward BPNN models.

Table 10: Final optimization results of PMEDM process in different machining regimes.

Setting level	Optimal Ra and MRR parameters				
	A-MRR	E-MRR	P-MRR	E-Ra	P-Ra
C_p 9%, T_{ON} 16 μs, T_{OFF} 30 μs, I_p 10 A, and V_S 5 V	5.903	6.113	6.192	1.695	1.735
Relative error (%)	3.43		1.29		2.35

values of E-MRR, P-MRR and E-Ra, and P-Ra are illustrated in Figures 9 and 10, respectively.

Figure 11 demonstrates the performance comparison of the obtained MRR values using FEM and experimental and proposed scalable conjugate-based feed forward BPNN models. It shows the values of A-MRR, E-MRR, and P-MRR are quite similar with lesser error values. Final confirmation test results are demonstrated in Table 10, where the values of A-MRR and E-MRR are compared with the obtained P-MRR using ANN model at an optimal combination of input process parameters with C_p 9%, T_{ON} 16 μs, T_{OFF} 30 μs, I_p 10 A, and V_S 5 V. Similarly, Ra was also compared at same combination of input process variables. In addition, relative error also computed for disclosing the significance of FEM analysis and ANN model with lesser than 4% of error.

6. Conclusion

This article addressed an investigation on PMEDM process of SS630 grade using SiC that has been carried out to analyse its performance with the additives of favourable effects of mixing powder into dielectric fluid, where four input process variables such as C_P, I_p, V_S, and T are considered with two output response measures, i.e., E-MRR and E-Ra. In addition, FEM analysis is employed for finding the distribution of temperature, heat flux, and statistical error. Then, A-MRR is computed based on the values of temperature distribution on SS630 workpiece material. Further, BPNN model with feed-forward architecture is utilized for finding the optimal process parameter combination of input variables such as C_P, I_p, V_S, and T and measured the output responses as P-MRR and P-Ra. Finally, confirmation test results are presented in terms of MRR as A-MRR, E-MRR, and P-MRR and surface quality as E-Ra and P-Ra. It is found that the relative error is below 4%.

The following conclusions are derived using the simulation and validation results:

(1) In the process of PMEDM, ANN model effectiveness has been proved in predicting the values of both Ra and MRR.

(2) The optimal input conditions can synthesize using the ANOVA model appropriately in addition to the ANN for PMEDM.

(3) The MRR is maximized, and Ra is minimized by the optimal input settings subjecting to necessary process constraints.

Data Availability

The data used to support the findings of this study are included within the article.

Disclosure

This study was performed as a part of the employment of Dambi Dollo University, Ethiopia.

Conflicts of Interest

Authors declare that there are no conflicts of interest in publication.

References

[1] R. Atefi, N. Javam, A. Razmavar, and F. Teimoori, "The influence of EDM parameters in finishing stage on surface quality, MRR and EWR," *Research Journal of Applied Sciences, Engineering and Technology*, vol. 4, no. 10, pp. 1287–1294, 2012.

[2] S. Prabhu and B. K. Vinayagam, "Analysis of surface characteristics of AISI D2 tool steel material using Electric Discharge Machining process with Single wall carbon nano tubes," *International Journal of Engineering and Technology*, vol. 2, pp. 35–41, 2010.

[3] N. S. Khundrakpam, H. Singh, S. Kumar, and G. S. Brar, "Investigation and modeling of silicon powder mixed EDM using response surface method," *Int. J. Curr. Eng. Technol.*vol. 4, no. 2, pp. 1022–1026, 2014.

[4] B. Reddy, G. N. Kumar, and K. Chandrashekar, "Experimental investigation on process performance of powder mixed electric discharge machining of AISI D3 steel and EN-31 steel," *Int. J. Curr. Eng. Technol.*vol. 4, no. 3, pp. 1218–1222, 2014.

[5] H. Singh, "Experimental study of distribution of energy during EDM process for utilization in thermal models," *International Journal of Heat and Mass Transfer*, vol. 55, pp. 5053–5064, 2012.

[6] B. Izquierdo, J. A. Sanchez, S. Plaza, I. Pombo, and N. Ortega, "A numerical model of the EDM process considering the effect of multiple discharges," *International Journal of Machine Tools and Manufacture*, vol. 49, no. 3-4, pp. 220–229, 2009.

[7] T. Yih-fong and C. Fu-chen, "Investigation into some surface characteristics of electrical discharge machined SKD-11 using powder-suspension dielectric oil," *Journal of Materials Processing Technology*, vol. 170, pp. 385–391, 2005.

[8] A. Bhattacharya, A. Batish, and N. Kumar, "Surface characterization and material migration during surface modification of die steels with silicon, graphite and tungsten powder in EDM process," *Journal of Mechanical Science and Technology*, vol. 27, no. 1, pp. 133–140, 2013.

[9] B. Jabbaripour, M. H. Sadeghi, and M. R. Shabgard, "Investigating surface roughness, material removal rate and corrosion resistance in PMEDM of r-TiAl intermetallic," *Journal of Manufacturing Processes*, vol. 15, no. 1, pp. 158–166, 2013.

[10] H. M. Chow, B. H. Yan, and F. Y. Huang, "Study of added powder in kerosene for the micro-slit machining of titanium alloy using electro-discharge machining," *Journal of Materials Processing Technology*, vol. 101, no. 1, pp. 95–103, 2000.

[11] S. Padhee, N. Nayak, and S. K. Panda, "Multi-objective parametric optimization of powder mixed electro-discharge machining using response surface methodology and non-dominated sorting genetic algorithm," *Sadhana*, vol. 37, no. 2, pp. 223–240, 2012.

[12] G. S. Prihandana, "Application of powder suspended in dielectric fluid for fine finish micro-EDM of Inconel 718," *International Journal of Advanced Manufacturing Technology*, vol. 75, no. 1–4, pp. 599–613, 2014.

[13] M. M. Sari, M. Y. Noordin, and E. Brusa, "Evaluating the electrical discharge machining (EDM) parameters with using carbon nanotubes," *IOP Conference Series: Materials Science and Engineering*, vol. 40, Article ID 012019, 2012.

[14] C. J. L. Puertas and L. Alvarez, "Analysis of the influence of EDM parameters on surface quality, MRR and EW of WC–Co," *Journal of Materials Processing Technology*, vol. 153, pp. 1026–1032, 2004.

[15] B. Surekha, T. S. Lakshmi, H. Jena, and P. Samal, "Response surface modelling and application of fuzzy grey relational analysis to optimize the multi-response characteristics of EN-19 machined using powder mixed EDM," *Australian Journal of Mechanical Engineering*, vol. 19, no. 1, pp. 19–29, 2019.

[16] T. Tahsin, Y. Hamidullah, E. Nihal, and E. Bulent, "Particle migration and surface modification on Ti6Al4V in SiC powder mixed electrical discharge machining," *Journal of Manufacturing Processes*, vol. 31, pp. 744–758, 2018.

[17] L. Selvarajan, J. Rajavel, V. Prabakaran, B. Sivakumar, and G. Jeeva, "A review paper on EDM parameter of composite material and industrial demand material machining," *Proceedings, Mater. Today*, vol. 5, no. 2, pp. 5506–5513, 2018.

[18] S. D. Choudhury, N. J. Sahari, B. Surekha, and G. Mondal, "Study on the influence of hybridized powder mixed dielectric in electric discharge machining of alloy steels," *Materials Today: Proceedings*, vol. 5, no. 9, Article ID 18410, 2018.

[19] S. Kumar, A. K. Dhingra, and S. Kumar, "Parametric optimization of powder mixed electrical discharge machining for nickel-based superalloy inconel-800 using response surface methodology," *Mechanics of Advanced Materials and Modern Processes*, vol. 3, no. 7, 2017.

[20] A. Kumar, S. Kumar, A. Mandal, and A. R. Dixit, "Investigation of powder mixed EDM process parameters for machining Inconel alloy using response surface methodology," *Materials Today: Proceedings*, vol. 5, pp. 6183–6188, 2018.

[21] B. P. Mishra and B. C. Routaray, "Impact of induction hardened work piece hardness on EDM performance," *Materials and Manufacturing Processes*, vol. 33, no. 6, pp. 626–633, 2018.

[22] S. S. Sidhu and M. Yazdani, "Comparative analysis of MCDM techniques for EDM of SiC/A359 composite," *Arabian Journal for Science and Engineering*, vol. 43, pp. 1093–1102, 2018.

[23] R. Toshimitsu, A. Okada, R. Kitad, and Y. Okamoto, ""Improvement in surface characteristics by EDM with chromium powder mixed fluid," 18th CIRP conference on electro physical and chemical machining (ISEM XVIII)," *Procedia CIRP*, vol. 42, pp. 231–235, 2016.

[24] N. Ekmekci and B. Ekmekci, "Electrical discharge machining of Ti6Al4v in hydroxyapatite powder mixed dielectric liquid," *Materials and Manufacturing Processes*, vol. 31, no. 13, pp. 1663–1670, 2015.

[25] A. A. Khazraji, S. A. Amin, and S. M. Ali, ""The effect of SiC powder mixing electrical discharge machining on white layer thickness, heat flux and fatigue life of AISI D2 die steel," Engineering Science and Technology," *An International Journal*, vol. 19, 2016.

[26] A. Batish, A. Bhattacharya, and N. Kumar, ""Powder mixed dielectric: an approach for improved process performance in EDM", Particulate Science and Technology," *International Journal*, vol. 33, no. 2, pp. 150–158, 2015.

[27] A. Kuriachen and J. Mathew, "Effect of powder mixed dielectric on material removal and surface modification in micro electric discharge machining of Ti-6Al-4V," *Materials and Manufacturing Processes*, vol. 31, no. 4, pp. 439–446, 2016.

[28] H. Baseri and S. Sadeghian, "Effects of nanopowder TiO2-mixed dielectric and rotary tool on," *EDM" International Journal of Advanced Manufacturing and Technology*, vol. 83, pp. 519–528, 2016.

[29] S. Tripathy and D. K. Tripathy, ""Multi-attribute optimization of machining process parameters in powder mixed electro-discharge machining using TOPSIS and grey relational analysis", Engineering Science and Technology," *An International Journal*, vol. 19, no. 1, pp. 62–70, 2016.

[30] G. S. Prihandana, T. Sriani, M. Mahardika et al., "Application of powder suspended in dielectric fluid for fine finish micro-EDM of Inconel 718," *International Journal of Advanced Manufacturing Technology*, vol. 75, pp. 599–613, 2014.

[31] V. N. R. Jampana and P. S. V. Ramana Rao, "Experiemntal Investigation and Optimization of Die-Sinking EDM of Grade 630 Stainless Steel Using Taguchi Approach," *Metrialtoday: proceedings*, 2021.

[32] A. Upadhyay and V. Sharma, "Optimizing material removal rate using artificial neural network for micro-EDM," *Design and Optimization of Mechanical Engineering Products*, pp. 209–233, 2018.

[33] H. Payal, S. Maheswari, and P. S. Bharti, "Process modelling of electric discharge machining of Inconel 825 using artificial neural networks," *International Journal of Mechanical & Mechatronics Engineering*, vol. 11, no. 3, pp. 562–566, 2017.

[34] J. Singh and R. K. Sharma, "Modelling and optimization of multi-performance characteristics of powder-mixed EDM of tungsten carbide alloy using intelligent decision-making tools," vol. 16, no. 2, pp. 101–128, 2017.

[35] M. Quarto, C. G. Urso, G. Maccarini, and M. Carminati, "A comparison between finite element model (fem) simulation and an integrated artificial neural network (ANN)-particle swarm optimization (PSO) approach to forecast performances of micro electro discharge machining (micro-EDM) drilling," *Micromachines*, vol. 12, no. 6, p. 667, 2021.